Computers and Chemical Engineering 172 (2023) 108171

Contents lists available at ScienceDirect

Computers and Chemical Engineering

journal homepage: www.elsevier.com/locate/cace

Demand response for flat nonlinear MIMO processes using dynamic ramping constraints

Florian Joseph Baader [a,b,c,*], Philipp Althaus [a,c], André Bardow [a,b], Manuel Dahmen [a]

[a] Forschungszentrum Jülich GmbH, Institute of Energy and Climate Research, Energy Systems Engineering (IEK-10), 52425 Jülich, Germany
[b] ETH Zürich, Energy & Process Systems Engineering, Zürich 8092, Switzerland
[c] RWTH Aachen University, Aachen, 52062, Germany

ARTICLE INFO

Keywords:
Demand response
Mixed-integer dynamic optimization
Flatness
Simultaneous scheduling

ABSTRACT

Volatile electricity prices make demand response attractive for processes that can modulate their production rate. However, if nonlinear dynamic processes must be scheduled simultaneously with their local multi-energy system, the resulting scheduling optimization problems often cannot be solved in real time. For single-input single-output processes, the problem can be simplified without sacrificing feasibility by dynamic ramping constraints that define a derivative of the production rate as the ramping degree of freedom. In this work, we extend dynamic ramping constraints to flat multi-input multi-output processes by a coordinate transformation that gives the true nonlinear ramping limits. Approximating these ramping limits by piecewise affine functions gives a mixed-integer linear formulation that guarantees feasible operation. As a case study, dynamic ramping constraints are derived for a heated reactor-separator process that is subsequently scheduled simultaneously with its multi-energy system. The dynamic ramping formulation bridges the gap between rigorous process models and simplified process representations for real-time scheduling.

1. Introduction

Reducing greenhouse gas emissions requires increased renewable electricity production that, however, gives a fluctuating supply. This fluctuating supply can be compensated by consumers that react to time-varying electricity prices by shifting their demand in time in a so-called demand response (DR) (Zhang and Grossmann, 2016). DR can be attractive for energy-intensive production processes with the flexibility to modulate their production rate. To exploit the DR potential, a scheduling optimization is needed, which typically determines operational set-points for a time horizon in the order of one day (Baldea and Harjunkoski, 2014). However, such a scheduling optimization is computationally challenging for nonlinear processes that exhibit scheduling-relevant dynamics. The scheduling optimization becomes even more difficult if processes do not only consume electricity but also heating or cooling as these processes need to be scheduled simultaneously with the local multi-energy supply system (often also referred to as utility system) (Leenders et al., 2019). Local multi-energy supply systems bring integer on/off decisions into the scheduling optimization, especially as they often consist of multiple redundant units (Voll et al., 2013). Thus, the simultaneous scheduling optimization problem usually is a nonlinear mixed-integer dynamic optimization (MIDO) problem (Baader et al., 2022c).

Traditionally, such challenging scheduling MIDO problems are simplified by introducing static ramping constraints that define the rate of change of the production rate ρ as degree of freedom ν and limit ν with constant ramping limits $\nu^{\min}$, $\nu^{\max}$, see e.g., (Carrion and Arroyo, 2006; Mitra et al., 2012; Adamson et al., 2017; Hoffmann et al., 2021; Zhou et al., 2017):

$$\dot{\rho} = \nu \text{ with } \nu^{\min} \leq \nu \leq \nu^{\max} \tag{1}$$

If additionally, the nonlinear energy demand of the production process is approximated as a piecewise-affine (PWA) function, the complete problem can be reformulated as a mixed-integer linear program (MILP) (Schäfer et al., 2020).

Traditional ramping constraints, however, have two shortcomings: They are restricted to (i) first-order dynamics and (ii) constant ramping limits. To tackle both shortcomings, we proposed high-order dynamic ramping constraints in our previous publication (Baader et al., 2022a). These high-order dynamic ramping constraints limit the δ-th derivative of the production rate ρ and use limits $\nu^{\min}$, $\nu^{\max}$ which are functions of the production rate and its time derivatives:

$$\rho^{(\delta)} = \nu \text{ with } \nu^{\min}\left(\rho, \dot{\rho}, \ldots, \rho^{(\delta-1)}\right) \leq \nu \leq \nu^{\max}\left(\rho, \dot{\rho}, \ldots, \rho^{(\delta-1)}\right) \tag{2}$$

* Corresponding author at: ETH Zürich, Energy & Process Systems Engineering, Zürich 8092, Switzerland.
E-mail address: fbaader@ethz.ch (F.J. Baader).

https://doi.org/10.1016/j.compchemeng.2023.108171
Received 11 July 2022; Received in revised form 26 October 2022; Accepted 7 February 2023
Available online 15 February 2023

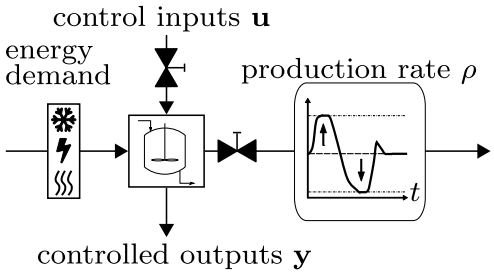

Fig. 1. A MIMO process that can vary its production rate ρ and thus its energy demand while additional control inputs **u** are available to control further process outputs variables **y**.

Dynamic ramping constraints allow to represent energy-intensive processes better than static ones due to their ability to account for high-order dynamics and non-constant ramping limits that depend on the process state. In Baader et al. (2022a), we demonstrated that dynamic ramping constraints can achieve solutions of the scheduling optimization problem that are close to the solutions of the original nonlinear MIDO problem while allowing to formulate MILPs that can be solved sufficiently fast for real-time scheduling. Moreover, we presented a method to derive dynamic ramping constraints rigorously for the special case of single-input single-output (SISO) processes that are exact input-state linearizable. However, this case is quite restrictive, and the question remained how to derive dynamic ramping constraints for more general processes. In particular, it was open how to apply the dynamic ramping method to multi-input multi-output (MIMO) processes that have a variable production rate ρ while, at the same time, other output variables **y** such as temperatures and concentrations need to be controlled using a set of control inputs **u** (Fig. 1).

The present publication extends the dynamic ramping approach to MIMO processes and presents a method to derive dynamic ramping constraints rigorously for differentially flat MIMO processes. In simple words, a MIMO process with m inputs is differentially flat if an output vector ξ of the same size m exists such that all process states and inputs can be given as a function of the output ξ and its β time derivatives $\dot{\xi}$, $\ldots$, $\xi^{(\beta)}$ (Fliess et al., 1995; Rothfuß, 1997; Rothfuß et al., 1996). We make use of the fact that a flat nonlinear model can be transformed to a linear model (Fliess et al., 1995). However, constraints that are linear for the original model, e.g., bounds on inputs, are nonlinear for the transformed model. In other words, a nonlinear model with linear constraints is transformed into a linear model with nonlinear constraints. Approximating the nonlinear bounds to the safe side with piecewise-affine functions allows us to formulate a MILP, whose solution is guaranteed to be feasible also for the non-approximated version. Note that for SISO processes, flatness is equivalent to exact input-state linearizability (Adamy, 2014), which was the main assumption in our previous work (Baader et al., 2022a). For MIMO processes, exact input-state linearizability with static state transformation is a special case of flatness (Adamy, 2014).

The remaining paper is structured as follows: In Section 2, the considered demand response optimization problem and the dynamic ramping constraints are introduced. In Section 3, a method is presented to derive dynamic ramping constraints for flat MIMO processes. In Section 4, a case study is presented. Section 5 provides further discussion and Section 6 concludes the work.

2. Dynamic mixed-integer linear scheduling with ramping constraints

This section briefly introduces the simultaneous scheduling optimization problem (P) of flexible processes represented by dynamic ramping constraints and multi-energy supply systems. This problem is a mixed-integer dynamic optimization (MIDO) problem with linear and piecewise affine (PWA) functions. We discretize time through collocation on finite elements (Biegler, 2010) to convert the MIDO problem (P) to a MILP. The size of the final MILP problem is proportional to the number of discretization points. Note that all decision variables $\chi = \left(\nu, (\mathbf{Q}_{\text{dem}}^{\text{process}})^T, \rho, S, \Phi_{\text{energy}}, (\mathbf{Q}^{\text{in}})^T, (\mathbf{Q}^{\text{out}})^T, (\Delta\mathbf{P})^T, \mathbf{z}_{\text{on}}^T\right)^T$, which are introduced in the following, are functions of time t. Still, we do not state time dependency explicitly to ease readability. The problem (P) without time discretization reads:

$$\min_{\chi \in [\chi^l, \chi^u]} \quad \Phi_{\text{energy}}(t_f) \tag{Pa}$$

s.t. Dynamic ramping constraints (Pb)

Process energy demand model (Pc)

Product storage: $\dot{S} = \rho - \rho^{\text{nom}} \quad \forall t \in \mathbb{T}$ (Pd)

Energy costs: $\dot{\Phi}_{\text{energy}} = \sum_{e \in \mathbb{E}} p_e \left(\sum_{i \in \mathbb{C}_e^{\text{cons}}} Q_i^{\text{in}} + \Delta P_e \right) \quad \forall t \in \mathbb{T}$ (Pe)

Energy conversion: $Q_i^{\text{out}} = h_{Q_i^{\text{out}}}^{\text{PWA}}(Q_i^{\text{in}}) \quad \forall i \in \mathbb{C}, \ \forall t \in \mathbb{T}$ (Pf)

Minimum part-load : $z_i^{\text{on}} Q_i^{\min} \le Q_i^{\text{out}} \le z_i^{\text{on}} Q_i^{\max}, \quad \forall i \in \mathbb{C}, \ \forall t \in \mathbb{T}$ (Pg)

Balances: $Q_{\text{dem},e}^{\text{process}} + Q_{\text{dem},e}^{\text{inflexible}} = \sum_{i \in \mathbb{C}_e^{\text{sup}}} Q_i^{\text{out}} + \Delta P_e, \quad \forall e \in \mathbb{E}, \ \forall t \in \mathbb{T}$ (Ph)

The objective is to minimize the cumulative energy costs Φ_{energy} at final time t_f. The lower and upper bounds of the decision variables are χ^l and χ^u. In the following paragraph, we discuss the dynamic ramping constraints (Pb) and the process energy demand model (Pc) in detail. The remaining constraints (Pd) to (Ph) are standard constraints (Schäfer et al., 2020; Sass et al., 2020) and discussed in more detail in our previous publication (Baader et al., 2022a). Thus, we only briefly introduce the symbols here. All decision variables are functions of time $t \in \mathbb{T}$ although not stated explicitly to ease readability. The product storage with level S is filled by the production rate ρ and emptied with the nominal production ρ^{nom} (Pd). The rate of change of the energy costs Φ_{energy} is the price of an energy form e, p_e times the input power Q_i^{in} of energy conversion units consuming e, $\mathbb{C}_e$, and the power exchanged with the grid ΔP_e. The set $\mathbb{E}$ in (Pe) covers all considered energy forms. For the energy conversion of a components i in the set of components $\mathbb{C}$, the output power Q_i^{out} is given as piecewise affine function $h_{Q_i^{\text{out}}}^{\text{PWA}}$ of the input power Q_i^{in} (Pf). Additionally, minimum part-load is modeled with a binary variable z_i^{on} to ensure the output power Q_i^{out} is either zero or between minimum part-load $Q_i^{\min}$ and maximum power $Q_i^{\max}$ (Pg). Finally, the energy balances state that the demands of the flexible process $Q_{\text{dem},e}^{\text{process}}$ and the demands of other inflexible processes $Q_{\text{dem},e}^{\text{inflexible}}$ have to be satisfied by the output Q_i^{out} of energy conversion units supplying energy e, collected in set $\mathbb{C}_e^{\text{sup}}$, and power from the grid ΔP_e (Ph).

In our previous publication (Baader et al., 2022a), we only derived dynamic ramping constraints (Pb) for processes with a single input. We, therefore, only had to constrain a single time derivative of the production rate ρ with order δ, which we defined as the ramping degree of freedom $\nu = \rho^{(\delta)}$. In the present contribution, we consider multiple inputs **u** and can potentially have constraints on all considered derivatives of the production rate $\rho^{(\gamma)}$ with $\gamma = 1, \ldots, \delta$ and the integer δ being the order of the highest time derivative that is constrained by input bounds. For instance, the bounds of input u_1 could directly limit the first derivative of the production rate, $\dot{\rho}$, whereas the bounds on input u_2 could limit the second derivative of the production rate, $\rho^{(2)}$, directly and only influence the first derivative, $\dot{\rho}$, through the integration. The generalized dynamic ramping constraints (DRCs) developed in this publication therefore read:

$$\rho^{(\delta)} = \nu \tag{DRCa}$$

$$\dot{\rho}^{\min}(\rho) \le \dot{\rho} \le \dot{\rho}^{\max}(\rho) \tag{DRCb}$$

$$\vdots$$

$$\left(\rho^{(\gamma)}\right)^{\min}\left(\rho, \dot{\rho}, \dots, \rho^{(\gamma-1)}\right) \le \rho^{(\gamma)} \le \left(\rho^{(\gamma)}\right)^{\max}\left(\rho, \dot{\rho}, \dots, \rho^{(\gamma-1)}\right) \tag{DRCc}$$

$$\vdots$$

$$\nu^{\min}\left(\rho, \dot{\rho}, \dots, \rho^{(\delta-1)}\right) \le \nu \le \nu^{\max}\left(\rho, \dot{\rho}, \dots, \rho^{(\delta-1)}\right) \tag{DRCd}$$

Still, only the highest considered time derivative ρ^{δ} is a degree of freedom and thus defined as the ramping degree of freedom ν.

The limits $\left(\rho^{(\gamma)}\right)^{\min}$, $\left(\rho^{(\gamma)}\right)^{\max}$ as well as $\nu^{\min}$, $\nu^{\max}$ are in general nonlinear functions that we derive by coordinate transformation (Section 3). To incorporate the dynamic ramping constraint into an MILP formulation, the true nonlinear limits are approximated by piecewise-affine (PWA) functions for all considered derivatives $\gamma = 1, \dots, \delta$ because PWA functions allow us to formulate a mixed-integer linear scheduling problem. These piecewise-affine functions need to be conservative such that they prohibit constraint violation with respect to the true nonlinear limits to guarantee that the chosen trajectory for ρ satisfies all bounds on inputs and states. Accordingly, the approximations of $\left(\rho^{(\gamma)}\right)^{\min}$ and $\nu^{\min}$ must always by greater than or equal to the true nonlinear limits and the approximations of $\left(\rho^{(\gamma)}\right)^{\max}$ and $\nu^{\max}$ must always be lower than or equal to the real nonlinear limits. Choosing the quality of the approximations allows us to explicitly balance the achievable flexibility range against the computational burden.

The process energy demand $Q_{\mathrm{dem},e}$ (cf. Eq. (Pc)) for an energy form e is modeled as a function of the production rate and its time derivatives:

$$Q_{\mathrm{dem},e}^{\mathrm{process}}\left(\rho, \dot{\rho}, \dots, \rho^{(\delta-1)}, \nu\right) \tag{3}$$

Similar to the DRC, a piecewise-affine function is chosen for $Q_{\mathrm{dem},e}^{\mathrm{process}}$ to achieve an MILP formulation.

The problem formulation (P) with DRCs captures a larger share of the dynamic flexibility range of processes than static ramping constraints can do while still allowing to formulate a mixed-integer linear program. However, to choose suitable piecewise-affine ramping limits, the true nonlinear limits of the process need to be derived or approximated. In the following section, we show how these limits can be derived rigorously for MIMO processes that are differentially flat.

3. Deriving dynamic ramping constraints

In Section 3.1, necessary assumptions are stated and then our approach is presented in Section 3.2.

3.1. Assumptions

1. The process degrees of freedom are divided into a control input vector $\mathbf{u}$ and the variable production rate ρ. The process model is a system of ordinary differential equations given by:

   $$\dot{\mathbf{x}} = \mathbf{f}(\mathbf{x}, \mathbf{u}, \rho) \tag{4}$$

   with state vector $\mathbf{x} \in \mathbb{R}^n$, and a nonlinear right-hand side function $\mathbf{f}(\mathbf{x}, \mathbf{u}, \rho)$. We assume that there are no further inputs or disturbances to the process.
2. The control input vector $\mathbf{u}$, and the production rate ρ are bounded by minimum and maximum values $\mathbf{u}^{\min}$, $\mathbf{u}^{\max}$, and $\rho^{\min}$, $\rho^{\max}$, respectively. Similarly, the states $\mathbf{x}$ have to be maintained within bounds $\mathbf{x}^{\min}$, $\mathbf{x}^{\max}$.
3. The process (4) is flat. That is, the process has one or multiple flat output vectors $\boldsymbol{\xi}$. An output vector $\boldsymbol{\xi}$ is flat if it satisfies three conditions (Fliess et al., 1995; Rothfuß, 1997; Rothfuß et al., 1996):

   (a) The flat output vector can be given as a function $\boldsymbol{\phi}$ of states $\mathbf{x}$, inputs $\mathbf{u}$, production rate ρ, and time derivatives of $\mathbf{u}$ and ρ:

   $$\boldsymbol{\xi} = \boldsymbol{\phi}\left(\mathbf{x}, \mathbf{u}, \dot{\mathbf{u}}, \dots, \mathbf{u}^{(\alpha)}, \rho, \dot{\rho}, \dots, \rho^{(\kappa)}\right) \tag{5a}$$

   with finite integer numbers α, κ. The function $\boldsymbol{\phi}$ can be seen as a transformation from the original state and input space to the flat output space. Often, it is possible to choose flat outputs that have a physical meaning, e.g., the conversion of a reactor, and that are a function of the states $\mathbf{x}$ only (Adamy, 2014).

   (b) A backtransformation from the flat output and its derivatives to the original states $\mathbf{x}$ and inputs $\mathbf{u}$ can be found. Accordingly, the system states $\mathbf{x}$ and inputs $\mathbf{u}$ can be given as functions $\boldsymbol{\psi}_1$, $\boldsymbol{\psi}_2$ of the flat outputs $\boldsymbol{\xi}$, the production rate ρ, and a number of time derivatives of $\boldsymbol{\xi}$ and ρ:

   $$\mathbf{x} = \boldsymbol{\psi}_1\left(\boldsymbol{\xi}, \dot{\boldsymbol{\xi}}, \dots, \boldsymbol{\xi}^{(\beta-1)}, \rho, \dot{\rho}, \dots, \rho^{(\zeta-1)}\right) \tag{5b1}$$

   $$\mathbf{u} = \boldsymbol{\psi}_2\left(\boldsymbol{\xi}, \dot{\boldsymbol{\xi}}, \dots, \boldsymbol{\xi}^{(\beta)}, \rho, \dot{\rho}, \dots, \rho^{(\zeta)}\right) \tag{5b2}$$

   with finite integer numbers β, ζ.

   (c) The components of $\boldsymbol{\xi}$ are differentially independent (Rothfuß, 1997). Consequently, they do not fulfill any differential equation:

   $$\boldsymbol{\mu}(\boldsymbol{\xi}, \dot{\boldsymbol{\xi}}, \dots, \boldsymbol{\xi}^{(\beta)}) = \mathbf{0} \tag{5c}$$

   Condition (5c) is satisfied if condition (5b) is satisfied, $\dim(\boldsymbol{\xi}) = \dim(\mathbf{u}) = m$, and $\operatorname{rank}\left(\frac{\partial \mathbf{f}(\mathbf{x},\mathbf{u},\rho)}{\partial \mathbf{u}}\right) = m$, where m is the number of inputs (Rothfuß, 1997).

   Note: To check conditions (5a)–(5c), a candidate for a flat output vector $\boldsymbol{\xi}$ is needed. We assume that such a candidate for a flat output vector $\boldsymbol{\xi}$ can be identified based on engineering intuition.
4. The trajectory of the production rate ρ is determined by the scheduling optimization. Subsequently, the control input vector $\mathbf{u} \in \mathbb{R}^m$ is calculated by an underlying process control.

The flatness-based coordinate transformation is visualized in Fig. 2. A nonlinear model with linear constraints is transformed into a linear model with nonlinear constraints. The number of control degrees of freedom is maintained: While, in the original model, the m inputs u_k ($k = 1, \dots, m$) are the degrees of freedom, in the linear model, the m highest time derivatives of the output components $\xi_k^{(\beta_k)}$ ($k = 1, \dots, m$) are the degrees of freedom (Adamy, 2014; Fliess et al., 1995). The number of time derivatives β_k can deviate between the flat output components ξ_k (Adamy, 2014; Fliess et al., 1995). In the linear model, the transformed state vector $\boldsymbol{\Xi}$ is formed by the outputs and their time derivatives (except for the highest time derivative):

$$\boldsymbol{\Xi} = \left(\xi_1, \dots, \xi_1^{(\beta_1-1)}, \xi_2, \dots, \xi_2^{(\beta_2-1)}, \dots, \xi_m, \dots, \xi_m^{(\beta_m-1)}\right)^T \tag{6}$$

The dimension of the transformed state vector $\boldsymbol{\Xi}$ is greater or equal to the dimension of the original state vector $\mathbf{x}$ (Adamy, 2014; Fliess et al., 1995). Consequently, the original nonlinear process model is converted to a linear model consisting of m integrator chains. In the linear model, every flat output ξ_k can be varied with a β_k-th order dynamic independently of the other flat outputs. Note that flatness is a sufficient condition for controllability of a nonlinear process (Adamy, 2014).

To ease notation in the following, we introduce the ramping state vector

$$\boldsymbol{\varphi} = \left(\rho, \dot{\rho}, \dots, \rho^{(\delta-2)}, \rho^{(\delta-1)}\right)^T \tag{7}$$

and its time derivative

$$\dot{\boldsymbol{\varphi}} = \left(\dot{\rho}, \rho^{(2)}, \dots, \rho^{(\delta-1)}, \nu\right)^T. \tag{8}$$

3.2. Approach

The steps to derive dynamic ramping constraints further discussed in the following subsections are summarized in Fig. 3: First, a candidate for a flat output vector is selected based on two necessary flatness conditions (Section 3.2.1). Assuming this candidate is, in fact, a flat

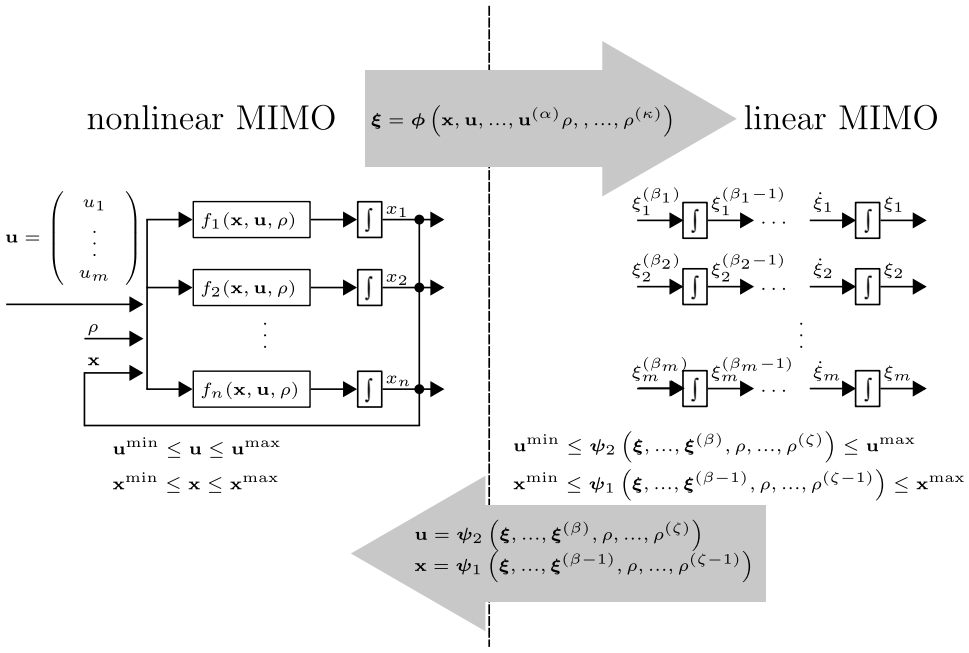

Fig. 2. Visualization of flatness-based coordinate transformation showing original nonlinear MIMO process model as introduced in assumption 1 (left), transformations $\boldsymbol{\phi}, \boldsymbol{\psi}_1, \boldsymbol{\psi}_2$ as introduced in assumption 3 (gray arrows), and linear MIMO process model in transformed coordinate space as introduced in assumption 3 (right).

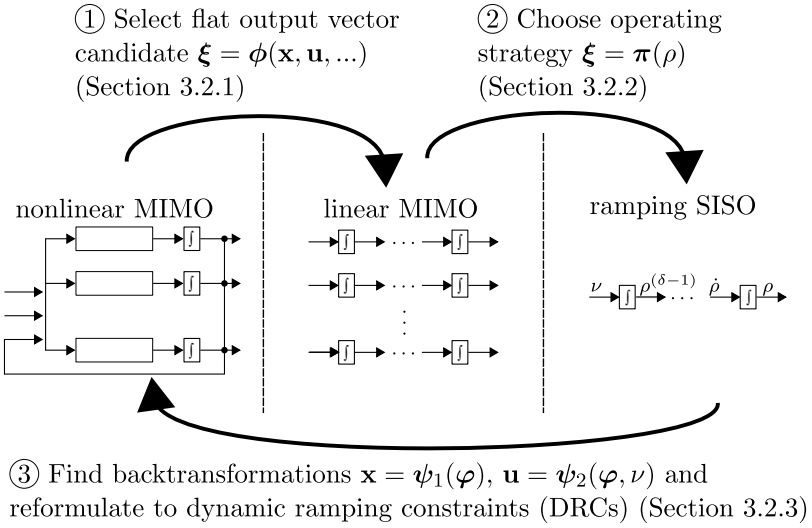

Fig. 3. Overview of steps to derive dynamic ramping constraints performed in the respective sections. For the nonlinear MIMO model and the linear MIMO model, all variable symbols are omitted for clarity as they are identical to Fig. 2. The variables of the ramping SISO model are the production rate ρ, its derivatives $\dot{\rho}, \ldots, \rho^{(\delta-1)}$, and the ramping degree of freedom ν.

output, the original nonlinear MIMO process model is transformed into a linear MIMO model (center of Fig. 3). In this linear model, the m components of the flat output vector ξ_k are decoupled such that the outputs ξ_k can be controlled independently of each other by manipulating the degrees of freedom $\xi_k^{(\beta_k)}$ (Fig. 2). However, a SISO model is needed for the dynamic ramping constraints where the production rate ρ is controlled by manipulating the ramping degree of freedom ν. Thus, second, the flat output components ξ_k are coupled by choosing an operating strategy $\boldsymbol{\pi}(\rho)$ that defines every ξ_k as function of the production rate ρ (Section 3.2.2). This coupling reduces the number of degrees of freedom from m to one, leading to a significant model order reduction. Third, backtransformations are found from the ramping SISO model to the original nonlinear MIMO model, and thus flatness is proven (Section 3.2.3).

Based on the backtransformations and the ramping SISO model, the true nonlinear ramping limits are derived from the bounds on inputs $\mathbf{u}$ and states $\mathbf{x}$. After approximating the true nonlinear limits with piecewise-affine functions, the dynamic ramping constraints are complete and the problem (P) can be solved as MILP.

3.2.1. *Selection of flat output candidate and necessary flatness conditions*

First, we propose to apply a necessary condition for flatness from literature based on a graph representation of the process (Schulze and Schenkendorf, 2020) to identify a candidate for the flat output

vector $\boldsymbol{\xi}$ as $\boldsymbol{\phi}\left(\mathbf{x}, \mathbf{u}, \dot{\mathbf{u}}, \ldots, \mathbf{u}^{(\alpha)}, \rho, \dot{\rho}, \ldots, \rho^{(\kappa)}\right)$ (compare to condition (5a)). As the second necessary condition for flatness, we propose setting up an equation system that implicitly defines the backtransformation $\boldsymbol{\psi}$ (compare to condition (5b)) and check if this backtransformation equation system is structurally solvable.

For the graph representation, the process model is represented as a directed graph in which all states x_i and inputs u_k are represented as vertices v_{x_i} and v_{u_k}, respectively (Schulze and Schenkendorf, 2020). If $\frac{\partial f_i(\mathbf{x},\mathbf{u})}{\partial x_j}$ is non-zero, there is an edge from vertex v_{x_j} to vertex v_{x_i} (Schulze and Schenkendorf, 2020). In other words: If a state x_j acts on the derivative of another state x_i, an edge is drawn from x_j to x_i. Similarly, an edge from input u_k to state x_i exists, if $\frac{\partial f_i(\mathbf{x},\mathbf{u})}{\partial u_k}$ is non-zero. The necessary condition for a flat output vector $\boldsymbol{\xi}$ is that it must be possible to match the m output components ξ_i to the input components u_i such that there are m input–output pairs with pairwise disjoint paths through the graph that cover all process states (Schulze and Schenkendorf, 2020). An illustrative example for this necessary condition is given in the Supplementary Information (SI).

As a starting point, the states which are typically controlled can be tested as flat output candidates. Typical states to be controlled are outlet stream compositions, final effluent temperature, or the process hold-up (Jogwar et al., 2009).

Once a flat output vector candidate is identified based on the graph representation as $\boldsymbol{\xi} = \boldsymbol{\phi}(\mathbf{x}, \mathbf{u}, \dot{\mathbf{u}}, \ldots, \mathbf{u}^{(\alpha)}, \rho, \dot{\rho}, \ldots, \rho^{(\kappa)})$, condition 4a is fulfilled. Further, the rank criterion needed for condition 4c can be checked easily. As a final step to show flatness, existence of the backtransformations $\boldsymbol{\psi}_1, \boldsymbol{\psi}_2$ that give states $\mathbf{x}$ and inputs $\mathbf{u}$ as functions of the flat output $\boldsymbol{\xi}$ and its time derivatives $\dot{\boldsymbol{\xi}}, \ldots, \boldsymbol{\xi}^{(\beta)}$ needs to be shown (condition 4b). To obtain these backtransformations, a nonlinear system of equations needs to be developed with $\boldsymbol{\xi}$ and its derivatives $\dot{\boldsymbol{\xi}}, \ldots, \boldsymbol{\xi}^{(\beta)}$ on the right-hand side and left-hand side functions including the wanted quantities: states $\mathbf{x}$, inputs $\mathbf{u}$, and potentially derivatives of inputs. To set up the backtransformation, we make use of the fact that $\boldsymbol{\xi}$ is given by $\boldsymbol{\phi}\left(\mathbf{x}, \mathbf{u}, \dot{\mathbf{u}}, \ldots, \mathbf{u}^{(\alpha)}, \rho, \dot{\rho}, \ldots, \rho^{(\kappa)}\right)$ and the derivatives of $\boldsymbol{\xi}$ can be given as functions of $\mathbf{x}$, inputs $\mathbf{u}$, and derivatives of inputs by means of the total differential. The equation system for the backtransformation needs to be square such that there are as many equations as there are unknown states, inputs, and derivatives of inputs. We propose to check if this nonlinear equation system is structurally solvable by conducting an analysis similar to the structural index analysis for differential–algebraic equation systems (Unger et al., 1995) commonly used in process systems engineering. An example is given in the SI.

3.2.2. Operating strategy

Under the assumption that the flat output candidate identified as discussed in Section 3.2.1 is, in fact, a flat output, the nonlinear model can be transformed into a linear model. This linear model is a MIMO model with m degrees of freedom $\xi_i^{(\beta_i)}$ and m outputs ξ_i (Fig. 2). As discussed above, the linear MIMO is transferred to a SISO ramping model by coupling the flat output components. To this end, we insert an operating strategy that gives the value of every flat output as a function of the production rate ρ. This operating strategy differentiates between two possible types of flat output components: First, flat output components might have specifications that should be maintained constant, such as outlet stream compositions, final effluent temperature, and the process hold-up (Jogwar et al., 2009). Accordingly, the operating strategy is to hold such an output ξ_k constant at its nominal value such that $\xi_k = \xi_k^{\text{nom}}$ holds and thus all time derivatives are zero.

Second, flat output components may be unspecified. For instance, in our case study, one flat output component is a concentration for which no specifications are given. As every flat output component ξ_k corresponds to one control input, i.e., degree of freedom, u_k, if specifications are given for l outputs, and l is smaller than m, $m - l$ flat output components remain as degrees of freedom in steady-state. Thus, the $m - l$ free flat output component ξ_k can, in principle, be chosen to have any value in steady-state as long as no variable bounds are violated. To have the optimal steady-state operating points, we use a steady-state optimization to determine the optimal values ξ_k in advance as a function of the production rate ρ such that $\xi_k = \pi_k(\rho)$. For instance, the objective can be to find the steady-state operating points that minimize energy consumption. In our case study, we choose the flat output component such that the overall heat demand is minimal for steady-state points (Section 4).

The operating strategy $\pi_k(\rho)$ can be any nonlinear function. The only requirement is that the function $\pi_k(\rho)$ must be differentiable with respect to ρ sufficiently often so that all derivatives of ξ_k which are part of the backtransformation discussed in the previous section are defined by the total differential, e.g., $\dot{\xi}_k = \frac{\partial \pi_k(\rho)}{\partial \rho}\dot{\rho}$, $\xi_k^{(2)} = \frac{\partial \pi_k(\rho)}{\partial \rho}\rho^{(2)} + \frac{\partial^2 \pi_k(\rho)}{\partial \rho^2}\dot{\rho}^2$.

When all output components with specifications are maintained at their nominal values and a function $\pi_k(\rho)$ is chosen for all other output components, the operating strategy can be summarized as $\boldsymbol{\xi} = \boldsymbol{\pi}(\rho)$. Consequently, the flat output vector $\boldsymbol{\xi}$ and all relevant time derivatives $\boldsymbol{\xi}, \dot{\boldsymbol{\xi}}, \ldots, \boldsymbol{\xi}^{(\beta)}$ (compare to Eq. (5b)) are defined as function of the production rate ρ and a number of its time derivatives. The highest time derivative $\rho^{(\delta)}$ that occurs defines the order of the dynamic ramping constraint (DRC) and the ramping degree of freedom $\nu = \rho^{(\delta)}$. Consequently, the backtransformations $\boldsymbol{\psi}_1, \boldsymbol{\psi}_2$ discussed in the following only depend on the ramping state vector $\boldsymbol{\varphi}$ and the ramping degree of freedom ν.

3.2.3. Backtransformation and reformulation to dynamic ramping constraints

First, the flat output vector $\boldsymbol{\xi}$ and its time derivatives $\boldsymbol{\xi}, \dot{\boldsymbol{\xi}}, \ldots, \boldsymbol{\xi}^{(\beta)}$ are replaced in the nonlinear equation system for the backtransformation derived in Section 3.2.1. While $\boldsymbol{\xi}$ is replaced by $\boldsymbol{\pi}(\rho)$, the derivatives are replaced by building the total differential of $\boldsymbol{\pi}(\rho)$. Next, we solve the equation system to get $\mathbf{x} = \boldsymbol{\psi}_1(\boldsymbol{\varphi})$ and $\mathbf{u} = \boldsymbol{\psi}_2(\boldsymbol{\varphi}, \nu)$. It is favorable to solve the equation system analytically. Still, it is not necessary to derive the functions $\boldsymbol{\psi}_1, \boldsymbol{\psi}_2$ analytically as they can also be evaluated numerically as long as their solution is unique. In this paper, we use the computer algebra package SymPy (Meurer et al., 2017) to obtain analytic functions $\boldsymbol{\psi}_1, \boldsymbol{\psi}_2$. Note that it might not be possible to solve the system of equations because the graphical and structural criteria proposed in Section 3.2.1 are only necessary flatness conditions. In case the nonlinear system of equations cannot be solved, one can test other flat output candidates. If the functions $\boldsymbol{\psi}_1, \boldsymbol{\psi}_2$ are found, condition 3b is fulfilled, and flatness is shown at least locally on the subspace defined by the operating strategy.

This flat system constitutes one integrator chain with the degree of freedom ν that can be chosen arbitrarily at any point in time. Thus, mathematically, the production rate can be changed infinitely fast by choosing infinitely high values for ν. However, the real process control inputs $\mathbf{u}$ are bounded by maximum and minimum values (assumption 3), and therefore, dynamic ramping constraints (DRCs) are needed to ensure that the real process inputs are maintained within bounds.

To get the dynamic ramping constraints (DRCs), we consider the input bounds row by row. For the kth row, we get

$$u_k^{\min} \leq \psi_{2,k}(\rho, \dot{\rho}, \ldots, \rho^{(\gamma)}) \leq u_k^{\max}, \tag{9}$$

where ρ^{γ} is the highest time derivative needed to compute u_k. Eq. (9) implicitly limits ρ^{γ} for given $\rho, \dot{\rho}, \ldots, \rho^{(\gamma-1)}$. These limits can be given as an explicit function if it is possible to symbolically invert $\psi_{2,k}$ for the derivative ${\rho^{(\gamma)}}_k$ and thus derive an analytic function θ of the production rate ρ, derivatives $\dot{\rho}, \ldots, \rho^{\gamma-1}$, and the input u_k:

$${\rho^{(\gamma)}}_k = \theta\left(\rho, \dot{\rho}, \ldots, \rho^{\gamma-1}, u_k\right) \tag{10}$$

Inserting $u_k^{\min}$, $u_k^{\max}$ into θ gives ${\rho^{(\gamma)}}_k^{\min}$, ${\rho^{(\gamma)}}_k^{\max}$. Alternatively, the limits can be derived numerically for given $\rho, \dot{\rho}, \ldots, \rho^{\gamma-1}$ by sampling different values for ${\rho^{(\gamma)}}_k$ and evaluating if the resulting u_k is within the allowed range.

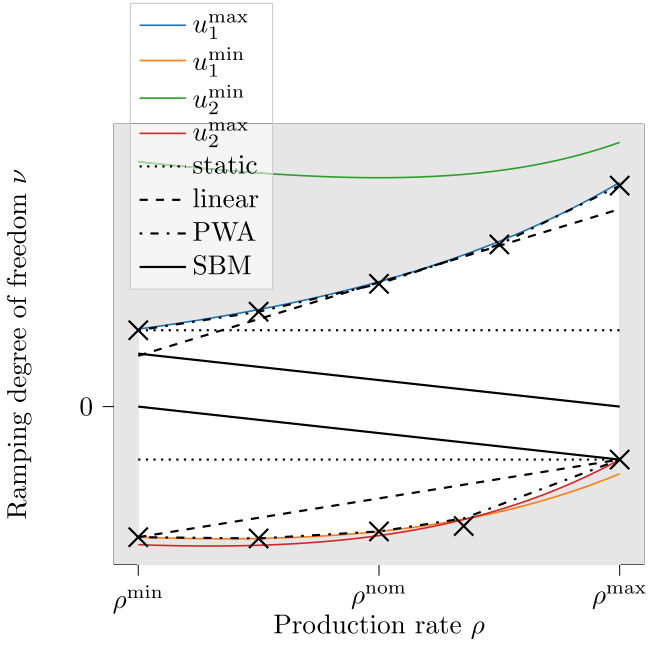

Fig. 4. Constraints for ramping degree of freedom ν as function of production rate ρ for an illustrative case with first-order ramping constraints and two limiting inputs u_1, u_2. For first-order ramping constraints, the ramping state vector $\boldsymbol{\varphi}$ is of dimension one and equal to the production rate ρ. Consequently, the limits on the ramping degree of freedom ν only depend on ρ. The true nonlinear limits caused by the minimum and maximum values of the two inputs u_1, u_2 are compared to static limits (dotted), linear limits (dashed) and piecewise-affine (PWA) limits (dashed–dotted). Moreover, a linear scale-bridging model (SBM) is visualized (compare to discussion in Section 3.3).

Note: Here, we discuss the case of one allowed region for ${\rho^{(\gamma)}}_k$ given by limits ${\rho^{(\gamma)}}_k^{\min}$, ${\rho^{(\gamma)}}_k^{\max}$. In principle, there could be two (or even more) non-connected allowed regions given by limits ${\rho^{(\gamma)}}_k^{\min,1}$, ${\rho^{(\gamma)}}_k^{\max,1}$ and ${\rho^{(\gamma)}}_k^{\min,2}$, ${\rho^{(\gamma)}}_k^{\max,2}$ with ${\rho^{(\gamma)}}_k^{\max,1} < {\rho^{(\gamma)}}_k^{\min,2}$, as $\psi_{2,k}$ is a general nonlinear function. In that case, one could either restrict the operating range to one of the two regions or introduce a binary variable that indicates which region is active. An illustrative example that can result in two allowed regions is given in the SI.

Bounds on a state x_k give an equation which is has the same structure as Eq. (9). Thus, constraints on states can be treated in the same way as constraints on inputs.

Finally, the nonlinear ramping limits need to be approximated by piecewise affine (PWA) functions. This approximation allows to explicitly balance the quality of the dynamic ramping constraints against the computational burden. In contrast to previous work (Baader et al., 2022a), there can more be several inputs and states limiting the same derivative of the production rate ρ for the MIMO case. Fig. 4 shows an illustrative case with first-order ramping and two limiting inputs u_1, u_2. The upper ramping limit is only determined by the maximum input $u_1^{\max}$ as the upper limit in the flat system resulting from $u_2^{\min}$ is always above the limit from $u_1^{\max}$. In contrast, the lower ramping limit is given by an intersection between the lower limits from $u_1^{\min}$ and $u_2^{\max}$, respectively. If static ramping limits are chosen, a large amount of the feasible region needs to be cut off for the illustrative case in Fig. 4 (horizontal dotted lines). In contrast, linear (dashed lines in Fig. 4) and piecewise affine (dashed–dotted lines in Fig. 4) limits allow to come closer to the true nonlinear limits and thus realize a larger flexibility range. For the lower ramping limit, piecewise affine limits can be realized without the addition of binary variables as the feasible region is convex. However, for the upper limit, the feasible region is non-convex and binary variables are needed, making the optimization more computationally challenging.

As, in the general case, the limit functions $\left(\rho^{(\gamma)}\right)^{\min}$, $\left(\rho^{(\gamma)}\right)^{\max}$ are multivariate functions, multivariate regression methods, e.g., hinging hyperplanes (Breiman, 1993; Adeniran and Ferik, 2017; Kämper et al., 2021), convex region surrogates (Zhang et al., 2016; Schweidtmann et al., 2021), or artificial neural networks with ReLU activation functions (Grimstad and Andersson, 2019; Lueg et al., 2021), can be used to find piecewise-affine approximations.

3.3. Comparison to other approaches

Finally, we compare our approach to two other relevant approaches that integrate scheduling and control by considering a simplified version of the process dynamics in scheduling: scale-bridging models (Du et al., 2015) and data-driven closed-loop models (Kelley et al., 2018). The difference between the two alternative approaches is that scale-bridging models explicitly adapt the underlying control to linearize the closed-loop response (Du et al., 2015) while data-driven closed-loop models identify the response of the process to a change of the set-point ρ_{SP} from data (Dias and Ierapetritou, 2016; Diangelakis et al., 2017; Burnak et al., 2018; Pattison et al., 2016). Thus, data-driven closed-loop models, in general, identify a nonlinear closed-loop response, and scale-bridging models rely on a linearization performed by the underlying control. This linearization can be achieved by exact input–output linearization control (Du et al., 2015), scheduling-oriented model-predictive control (Baldea et al., 2015), or by a combination of a set-point filter and tracking control (Baader et al., 2022c). For first-order dynamics, the linearized closed-loop response reads

$$\rho + \tau\dot{\rho} = \rho_{\text{SP}} \tag{11}$$

In Eq. (11), τ is a tunable time constant and ρ_{SP} is the set-point given to the underlying controller. That is, instead of the ramping degree of freedom ν, the set-point ρ_{SP} is the degree of freedom for the scheduling optimization. To compare the scale-bridging model to our dynamic ramping constraints, we rearrange Eq. (11) to calculate the maximum possible rate of change $\dot{\rho}^{\max}$ as a function of the maximum set-point $\rho_{SP}^{\max}$ and the minimum rate of change $\dot{\rho}^{\min}$ as a function of the minimum set-point $\rho_{SP}^{\min}$:

$$\dot{\rho}^{\max} = \frac{1}{\tau}(\rho_{SP}^{\max} - \rho) \tag{12}$$

$$\dot{\rho}^{\min} = \frac{1}{\tau}(\rho_{SP}^{\min} - \rho) \tag{13}$$

The resulting limits are visualized in Fig. 4 for the natural choice that the maximum set-point $\rho_{SP}^{\max}$ equals the maximum production rate $\rho^{\max}$ and the minimum set-point $\rho_{SP}^{\min}$ equals the maximum production rate $\rho^{\min}$. The time constant τ is chosen such that the rate of change $\dot{\rho}$ demanded by the scale-bridging model is always within limits. The flexibility range for the scale-bridging model has a parallelogram shape dictated by Eqs. (12) and (13). Our dynamic ramping constraints can always match this parallelogram shape by linear ramping limits $\nu^{\min}$, $\nu^{\max}$. Additionally, dynamic ramping constraints also allow choosing linear limits with another shape or even piecewise affine limits. Thus dynamic ramping constraints can consistently perform at least as well as linear scale-bridging models. Moreover, our analysis could be used to rigorously choose the time constant τ of the scale-bridging model.

As stated above, data-driven closed-loop models identify a nonlinear closed-loop response. Still, if piecewise affine functions approximate nonlinearities, a MILP formulation is possible, see, e.g., Kelley et al. (2018) who derive an MILP formulation for Hammerstein-Wiener models. Thus, data-driven closed-loop models are an alternative to our dynamic ramping constraints; in particular, they are still applicable if no mechanistic process model is available or the process is not flat. If a flat mechanistic process model is available, there are two conceptual differences between dynamic ramping constraints and data-driven closed-loop models: First, dynamic ramping constraints have the theoretical advantage that they can be derived rigorously such that the

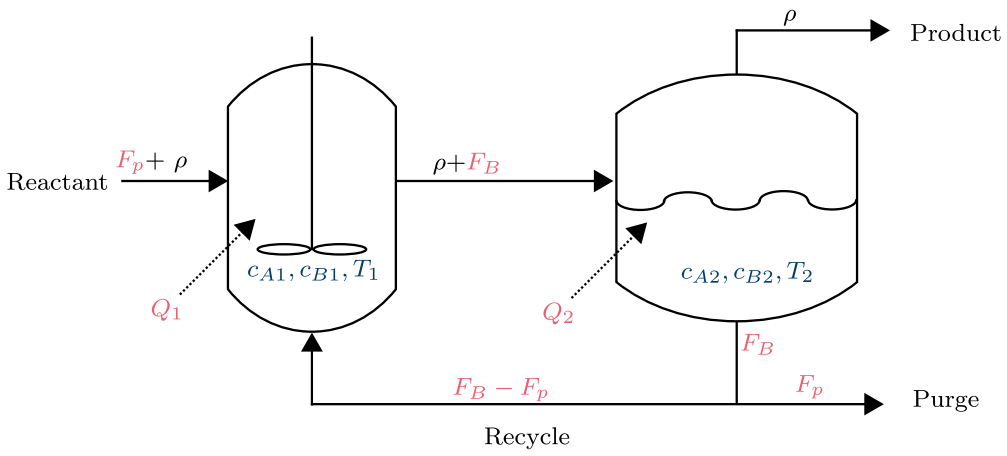

Fig. 5. Case study of reactor-separator process with recycle: States $\mathbf{x}$ are the concentrations of component A and B, c_A, and c_B, respectively, and the temperature T in the reactor (1) and in the flash (2). Manipulated control inputs $\mathbf{u}$ are the bottom stream F_B, the purge stream F_P, the heat input to the reactor Q_1, and the heat input to the flash Q_2. The scheduling degree of freedom is the production rate ρ. All other material flow rates are given as functions of F_B, F_p, and ρ, e.g., the reactant stream is equal to the purge F_p plus the production rate ρ as no accumulation of material occurs.

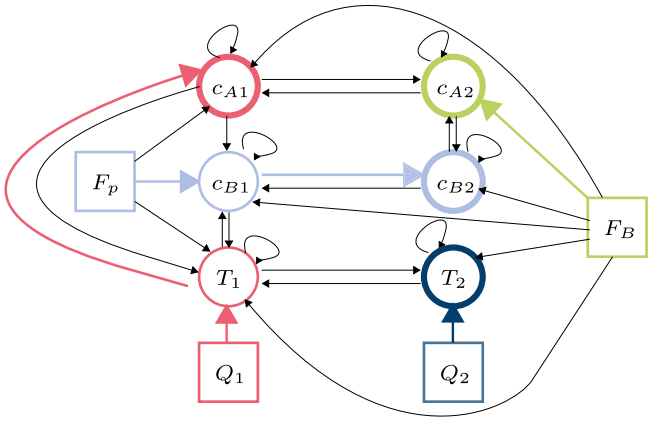

Fig. 6. Graph representation for the reactor-separator process with recycle (compare to Fig. 5). The output $\xi = (c_{A2}, c_{B2}, T_2, c_{A1})^T$ fulfills the necessary condition for a flat output.

feasibility of the optimized trajectory is guaranteed. Second, dynamic ramping constraints and data-driven closed-loop models lead to conceptually different trade-offs between computational burden and accuracy: While dynamic ramping constraints reduce the computational burden by reducing the accuracy of the ramping limits, data-driven closed-loop models reduce computational burden by reducing the accuracy of the model prediction. Thus, dynamic ramping constraints compromise on the feasible region, sacrificing flexibility, and data-driven closed-loop models compromise on the prediction of the process outputs, potentially leading to constraint violations or production deviating from the schedule.

4. Case study: Reactor-separator process with recycle

In this case study, we consider a reactor-separator process with recycle consisting of a continuous stirred tank reactor (CSTR) and a flash (Fig. 5). The production rate ρ can be varied around its nominal value ρ^{nom} between $\rho^{\text{min}} = 0.8\rho^{\text{nom}}$ and $\rho^{\text{max}} = 1.2\rho^{\text{nom}}$ as long as the nominal production is reached on average over the considered time horizon. A raw material A reacts to the desired product B, which can further react to an undesired product C. The process has 6 differential states: the concentration of A, c_{A1}, the concentration of B, c_{B1}, and the temperature T_1 in the reactor (1) and the analog quantities c_{A2}, c_{B2}, T_2, in the flash (2). Apart from the production rate ρ, there are four manipulated variables: the bottom stream F_B, the purge stream F_p, the heat flow to the reactor Q_1, and the heat flow to the flash Q_2. The process equations are modified from the textbook example by Christofides et al. (2011) where 2 CSTRs and a flash are considered. Though, also the original version (Christofides et al., 2011) fulfills our assumptions, we decided to modify the example to reduce the number of states from 9 to 6 to improve readability and clarity.

The model equations comprise component and energy balances given in the SI.

4.1. Selection of flat output candidate and necessary flatness conditions

A flat output candidate ξ must have 4 components as there are four control inputs. We first consider the three states of the flash c_{A2}, c_{B2}, and T_2, as they determine the outlet stream, and we assume that specifications for the outlet stream are given. As fourth output component, we choose the concentration c_{A1} based on the graph representation in Fig. 6. The four input–output pairs $F_B - c_{A2}$, $F_p - c_{B2}$, $Q_2 - T_2$, $Q_1 - c_{A1}$ fulfill the necessary condition for a flat output (Fig. 6).

By differentiating the components of the output $\xi = (c_{A2}, c_{B2}, T_2, c_{A1})$ up to three times, we receive a structurally solvable system of equations (Table S3 in the SI).

4.2. Operating strategy

For the operating strategy, we assume that the composition and temperature of the product stream ρ must be maintained constant. Accordingly, $\xi_1 = c_{A2}$, $\xi_2 = c_{B2}$, $\xi_3 = T_2$ must be maintained at their nominal values $\xi_1^{\text{nom}} = 0.4539$, $\xi_2^{\text{nom}} = 0.4610$, $\xi_3^{\text{nom}} = 455K$. Thereby, the considered operating region is already significantly reduced.

As there are 4 control inputs, we can maintain the first three flat output components at their nominal values and still have one degree of freedom left. Consequently, an operating strategy for the fourth flat output $\xi_4 = c_{A1}$ can be chosen freely. In a steady-state optimization, we search for the steady-state operating points that minimize the total heating $Q_1 + Q_2$ and fix ξ_4 to be a function of the production rate $\xi_4 = \pi_4(\rho)$. Further details on this steady-state optimization are given in the SI.

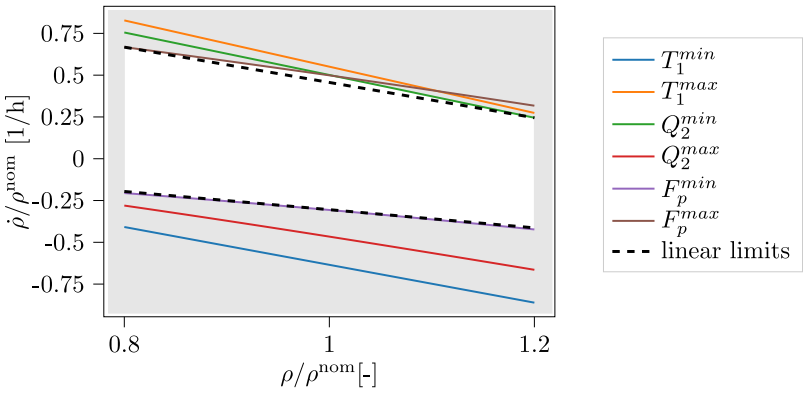

Fig. 7. Limits on the scaled time derivative of the production rate $\dot{\rho}$ over the scaled production rate ρ resulting from the minimum (min) and maximum (max) values of the state T_1 and the inputs F_p, Q_2.

Table 1
Structural dependency resulting from nonlinear transformation and operating strategy of states and inputs on the production rate ρ and its time derivatives $\dot{\rho}$ and ν $(= \rho^{(2)})$.

		ρ	$\dot{\rho}$	ν
States:	c_{A1}	x		
	c_{B1}	x		
	T_1	x	x	
	c_{A2} [a]			
	c_{B2} [a]			
	T_2 [a]			
Inputs:	F_B	x		
	F_p	x	x	
	Q_1	x	x	x
	Q_2	x	x	

[a]States which are held constant.

4.3. Reformulation to dynamic ramping constraints

After inserting the operating strategy defined in Section 4.2, we solve the nonlinear backtransformation equation system. To this end, we use the computer algebra package SymPy (Meurer et al., 2017) to find explicit algebraic expressions for all states and inputs, except for the temperature T_1. The temperature T_1 has to be determined numerically because the two reaction terms in the differential Equation (S9) lead to an equation of the form

$$0 = b_0 + b_1 e^{-\frac{E_1}{RT_1}} + b_2 e^{-\frac{E_2}{RT_1}}, \tag{14}$$

with parameters b_0, b_1, b_2. The implicit Eq. (14) has a unique solution for the temperature, as the exponential functions are monotonic. The numerical solution of Eq. (14) is found using the python package SciPy (Virtanen et al., 2020).

Table 1 provides the structural dependency of the states and inputs on the production rate ρ and its time derivatives $\dot{\rho}$ and ν $(= \rho^{(2)})$. The highest time derivative of the production rate that appears is two. Therefore, the ramping degree of freedom ν is equal to $\rho^{(2)}$. More detailed information about the reformulations is given in the SI.

For the dynamic ramping constraints, it has to be analyzed which state and input bounds limit the time derivatives of the production rate ρ. States and inputs that are either held constant or exclusively depend on the production rate ρ do not need to be checked because it is already known from the steady-state optimization that these variables take feasible values for all considered production rates. Consequently, the variables $c_{A,1}, c_{B,1}, c_{A,2}, c_{B,2}, T_2, F_B$ do not influence the dynamic ramping constraints (compare to Table 1).

The variables T_1, F_p, Q_2 depend on ρ and $\dot{\rho}$ but not on the second time derivative ν. Accordingly, the bounds of these variables limit the first time derivative $\dot{\rho}$. In Fig. 7, the limits on $\dot{\rho}$ resulting from variable bounds are shown over the production rate ρ. The calculation of these limits is explained in the SI. While the lower limit on $\dot{\rho}$ results from the bound $F_p^{\min}$, the upper limit is given by $F_p^{\max}$ for small production rates and by $Q_2^{\min}$ for large production rates. Graphically, we choose conservative linear functions for the limits $\dot{\rho}^{\min}(\rho) = a_0^{\min} + a_1^{\min}\rho$, $\dot{\rho}^{\max}(\rho) = a_0^{\max} + a_1^{\max}\rho$ with parameters $a_0^{\min}$, $a_1^{\min}$, $a_0^{\max}$, $a_1^{\max}$ (compare to (DRCb)).

The heating input Q_1 is the only variable that depends on the ramping degree of freedom ν. We choose piecewise affine limits $\nu_{\mathrm{PWA}}^{\min}(\rho, \dot{\rho})$, $\nu_{\mathrm{PWA}}^{\max}(\rho, \dot{\rho})$ (compare to (DRCd)) which cover 95% of the feasible area. Further details are given in the SI.

With the limits on ν, the second-order dynamic ramping constraints are completely parameterized and have the form:

$$\rho^{(2)} = \nu \tag{15}$$

$$a_0^{\min} + a_1^{\min}\rho \le \dot{\rho} \le a_0^{\max} + a_1^{\max}\rho \tag{16}$$

$$\nu_{\mathrm{PWA}}^{\min}(\rho, \dot{\rho}) \le \nu \le \nu_{\mathrm{PWA}}^{\max}(\rho, \dot{\rho}) \tag{17}$$

4.4. Investigation 1: Ramp optimizations

To illustrate the ramping behavior with the derived dynamic ramping constraints, we perform two as-fast-as-possible ramp optimizations shown in Fig. 8. The ramp-up from minimum production rate to maximum production rate takes 1.3 h, and the corresponding ramp-down takes 3.1 h. The ramp-up is first constrained by the acceleration, i.e., the bounds on ν, and then by the speed, i.e., the bounds on $\dot{\rho}$. In contrary, the ramp-down is always constrained by the bounds on ν.

To visualize such an optimized ramp on the full-order process model, we simulate the ramp-up by using the optimized production rate trajectory (left part of Fig. 8) as input to a simulation and calculate the control inputs $\mathbf{u}$ using the backtransformation function $\mathbf{u} = \boldsymbol{\psi}_2(\rho, \dot{\rho}, \nu)$ derived above. While the first three flat output components c_{A2}, c_{B2}, T_2 are maintained at their nominal values, the fourth output component c_{A1} follows the function of the production rate $c_{A1} = \pi_4(\rho)$ specified in the operating strategy (Fig. 9). All other states and inputs are within their respective bounds. Moreover, in the first half hour, when the ramp-up is limited by the limit on the acceleration $\nu^{\max}$ (compare to Fig. 8, left), Q_1 is close to its maximum value (Fig. 9) because the upper limit of $\nu^{\max}$ is derived from $Q_1^{\max}$. However, Q_1 does not reach its maximum value due to the conservative piecewise affine approximation. During the second half hour, the ramp-up is limited by the maximum speed $\dot{\rho}^{\max}$ (compare to Fig. 8, left) and thus the control input Q_2, which limits the speed for high production rates ρ (compare to Fig. 7), is close to its bounds (Fig. 9). Here, Q_2 comes very close to its bound as the conservative approximation of the ramping limit on $\dot{\rho}$ is very close to the true nonlinear limit (Fig. 7). Finally, at hour 1.25, the acceleration ν touches the lower limit $\nu^{\min}$ (Fig. 8) and the input Q_1 reaches its lower limit $Q_1^{\min}$ (Fig. 9).

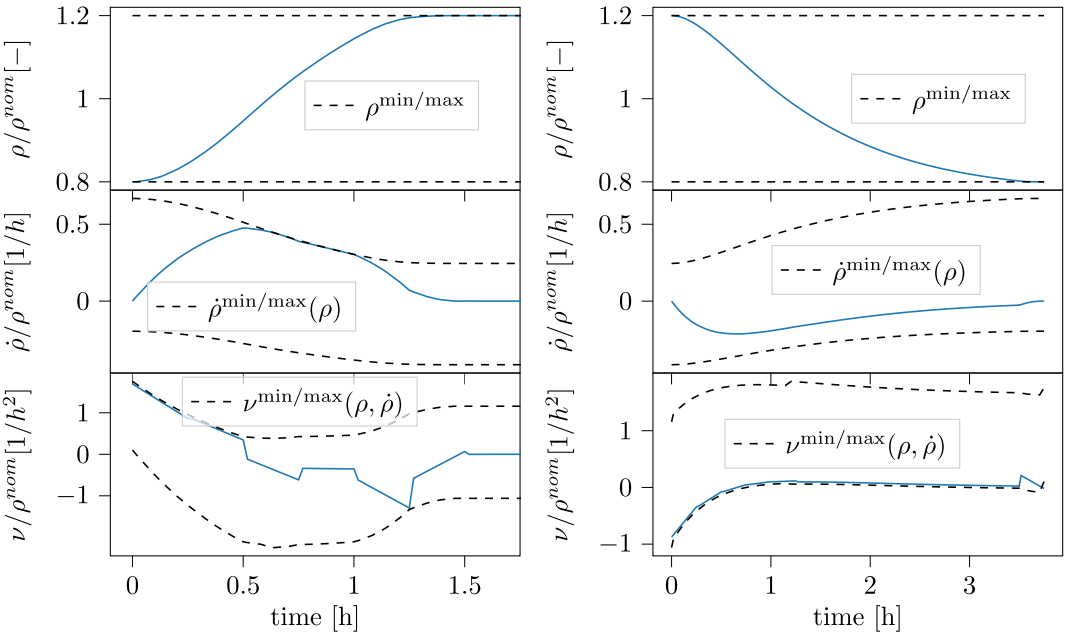

Fig. 8. Production rate ρ, its first time derivative $\dot{\rho}$, and ramping degree of freedom ν for an as-fast-as-possible ramp up (left) and an as-fast-as-possible ramp down (right) together with their bounds. The bounds of $\dot{\rho}$ are functions of ρ and the bounds of ν are functions of $\rho, \dot{\rho}$. The ramping degree of freedom ν is discretized to be piece-wise linear.

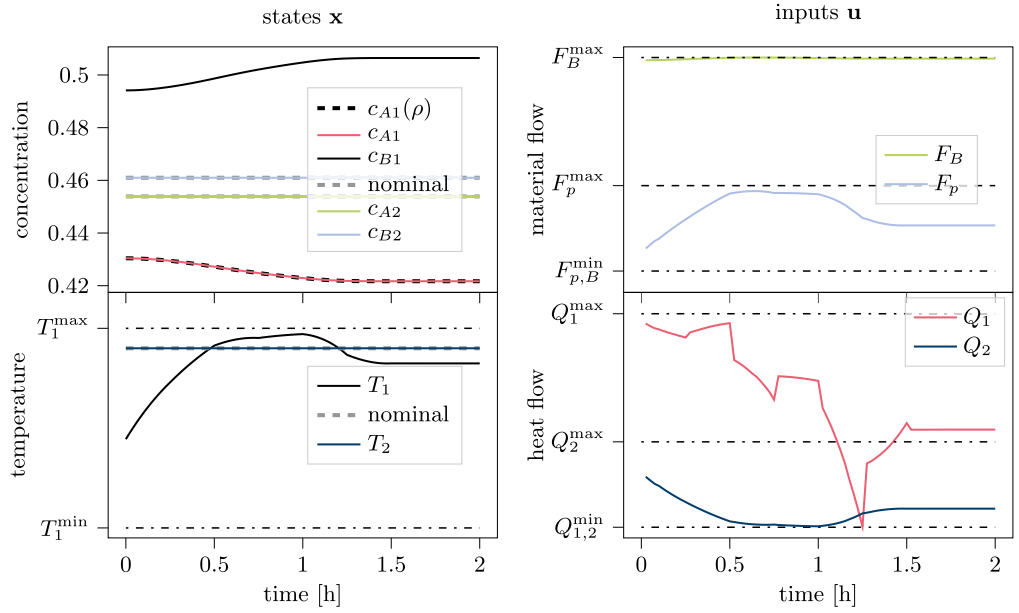

Fig. 9. Simulation result of ramp-up optimization (Fig. 8, left) on the full-order process model showing states $\mathbf{x} = (c_{A1}, c_{B1}, T_1, c_{A2}, c_{B2}, T_2)^T$ (left), and control inputs $\mathbf{u} = (F_B, F_p, Q_1, Q_2)^T$ (right). Minimum (min) and maximum (max) values are shown in dashed–dotted lines. The nominal values of the flat output components c_{A2}, c_{B2}, T_2 and the operating strategy $\pi_4(\rho)$ for the flat output component c_{A1} are shown in dashed lines.

Ramp optimization and corresponding simulation show that even though the dynamic ramping constraints are formed by linear and piecewise affine equations, they can capture dynamics that are significantly more complex than traditional static first-order ramps. Moreover, the original process model with 6 states and 5 degrees of freedom is reduced to a dynamic ramping constraint with only 2 states, i.e., ρ, $\dot{\rho}$, and one degree of freedom ν. Accordingly, coupling the flat outputs to the production rate reduces the model size and thus simplifies optimization.

4.5. Investigation 2: Demand response application

To demonstrate the dynamic ramping constraints in a DR application, the flexible process is considered together with a multi-energy

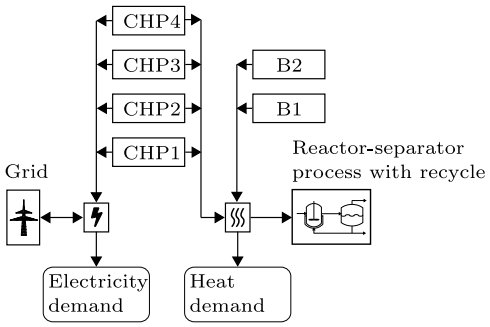

Fig. 10. Multi-energy system and reactor-separator process with recycle: The flexible process as well as additional non-flexible heat and electricity demands are supplied by an multi-energy system, consisting of 4 combined heat and power plants (CHP1-CHP4) and 2 boilers (B1, B2). Moreover, electricity can be exchanged with the grid.

system and additional non-flexible heat and electricity demands (Fig. 10). We consider an energy system based on Sass et al. (2020). However, instead of one combined heat and power plant (CHP) and one boiler (B), we extended the system to 4 CHPs and 2 boilers to study a larger energy system with more discrete on/off-decisions. Additionally, electricity can be bought from and sold to the grid for the day-ahead price that may change hourly. The details about the multi-energy system and the derivation of the optimization problem (P) are given in the SI.

The optimization problem (P) is formulated using pyomo (Hart et al., 2017, 2011) and discretized using the extension pyomo.dae (Nicholson et al., 2018). We apply discretization by orthogonal collocation on finite elements with 2 elements per hour and 3 collocation points per element. This discretization was found to be sufficiently accurate in preliminary calculations. Overall, we have 144 discretization points over the 24 h time horizon. The discretized problem has 5559 continuous variables. For the binary variables, we use a time discretization of one hour to match the time step of electricity prices. There are 6 binaries per hour for the on/off-decision of energy system units and 3 binaries per hour for the piecewise affine limits on the ramping degree of freedom ν and the piecewise affine energy demand model (more details in the SI). Thus, the final MILP problem has $9 \times 24 = 216$ binary variables.

The optimization problem is solved using gurobi version 9.5.2 (Gurobi Optimization, 2021). As Harjunkoski et al. (2014) state that the maximum acceptable optimization runtime for scheduling problems is typically between 5 and 20 min, we set the maximum optimization runtime to 5 min. All calculations are performed on a Windows 11 machine with an Intel(R) Core(TM) i7-1165G7 CPU and 16 GB RAM.

First, the energy system operation is optimized without accounting for the energy demand of the flexible process to obtain the energy costs of the inflexible demands only. Second, the operation of the energy system is optimized with the flexible process operating in steady-state such that the demand of the flexible process is constant (compare to Fig. 11, right). Third, the DR optimization is performed using dynamic ramping constraints (compare to Fig. 11, left).

The DR operation of the process reduces the total energy costs by 4.6% compared to steady-state operation. Considering only the energy costs associated with the flexible process, the cost reduction through demand response is 9.8%.

In the resulting operation, two types of periods can be distinguished: In times of low electricity prices, heat is preferably produced by the boilers, and electricity is bought from the grid (hours 13–18). In times of high electricity prices, heat is preferable provided by the CHPs, and excess electricity is sold to the grid (hours 1–12, 19–24). The DR case reduces costs due to two reasons: First, the boilers are operated less. Instead of 12 h, the boilers are only active in 10 h (Fig. 11). The amount of heat provided by the boilers is reduced by 2%. Second, the heat demand of the flexible process and, therefore, the electricity production of the CHPs is shifted from hours of low prices to hours with higher prices (Fig. 11). For instance, the heat demand is lower in hour 15 and higher in hour 5. Consequently, the derived dynamic ramping constraints allow to reduce costs substantially compared to steady-state process operation.

The optimization problem terminates after a maximum runtime of 5 min that we set following Harjunkoski et al. (2014). The remaining optimality gap is 3.9%. As a further comparison, we simplify the bounds of the ramping degree of freedom ν in Eq. (17) from piecewise affine to purely linear functions. These linear functions only cover 80% instead of 95% of the feasible area for ν (compare to Section 4.2). With these linear limits $\nu_{\text{lin}}^{\min}$, $\nu_{\text{lin}}^{\max}$, we receive very similar results compared to those previously obtained with the piecewise affine limits: While the cost reductions achieved with the linear limits slightly improve to 4.7% instead of 4.6%, the remaining optimality gap slightly worsens to 4.2% instead of 3.9%. That is, with purely linear dynamic ramping constraints, we find a comparable near-optimal solution with a comparable optimality gap. Overall, even if the on/off-status of 6 energy system units has to be optimized simultaneously with the process operation, the optimization provides a schedule achieving substantial cost reductions within this maximum optimization runtime of 5 min.

5. Discussion

In this section, we discuss possible adaptations and limitations of our approach.

Throughout this paper, we assume that the production rate ρ is a degree of freedom (compare to assumptions in Section 3.1). However, the method can be adapted to cases where the production rate is not a degree of freedom but a component of the flat output vector ξ_k. For instance, if the flow rate of the product stream would be hydraulically driven by a filling level h_{fill}, the production rate would be given as part of the flat output by a function of h_{fill}. In such cases, the production rate cannot be controlled directly but only through manipulating the corresponding input u_k. For instance, the filling level h_{fill} could be controlled by manipulating the feedflow of the corresponding unit.

In our operating strategy discussed in Section 3.2.2, all flat output components without given specifications are coupled to the production rate. This coupling reduces the dimensionality of the model. Instead of m flat outputs and their derivatives, only the production rate and its derivatives are variables in the optimization problem. Consequently, there are δ states and one degree of freedom. This dimensionality reduction strongly reduces the computational complexity of the optimization problem. Still, coupling all flat outputs with the production rate might be unfavorable in cases where some flat outputs can only be changed much slower than the production rate. In such cases, the outputs without specifications could be kept as independent integrator chains in the ramping model (right part in Fig. 3). In our case study, the concentration c_{A1}, which is the fourth flat output component, could be uncoupled such that there are two integrator chains in the ramping model: one for the production rate ρ and one for the concentration c_{A1}. Consequently, dynamic ramping constraints need to be derived for both integrator chains. While this uncoupled version makes the ramping model computationally more challenging, it is also more flexible and thus might enable higher profits in some cases. An extreme example is electrolyzers that can often adapt their production rate rapidly but have slow temperature dynamics (Simkoff and Baldea, 2020; Flamm et al., 2021). Thus, for electrolyzers, it is not favorable to couple the temperature with the production rate. Instead, we have shown recently in a conference paper that it is favorable to keep both production rate and temperature as degrees of freedom and formulate dynamic ramping constraints on the temperature (Baader et al., 2022b).

Conceptually, the electrolyzer example Baader et al. (2022b) also shows that it is possible to consider two scheduling-relevant variables at a time. Especially, our approach based on dynamic ramping constraints

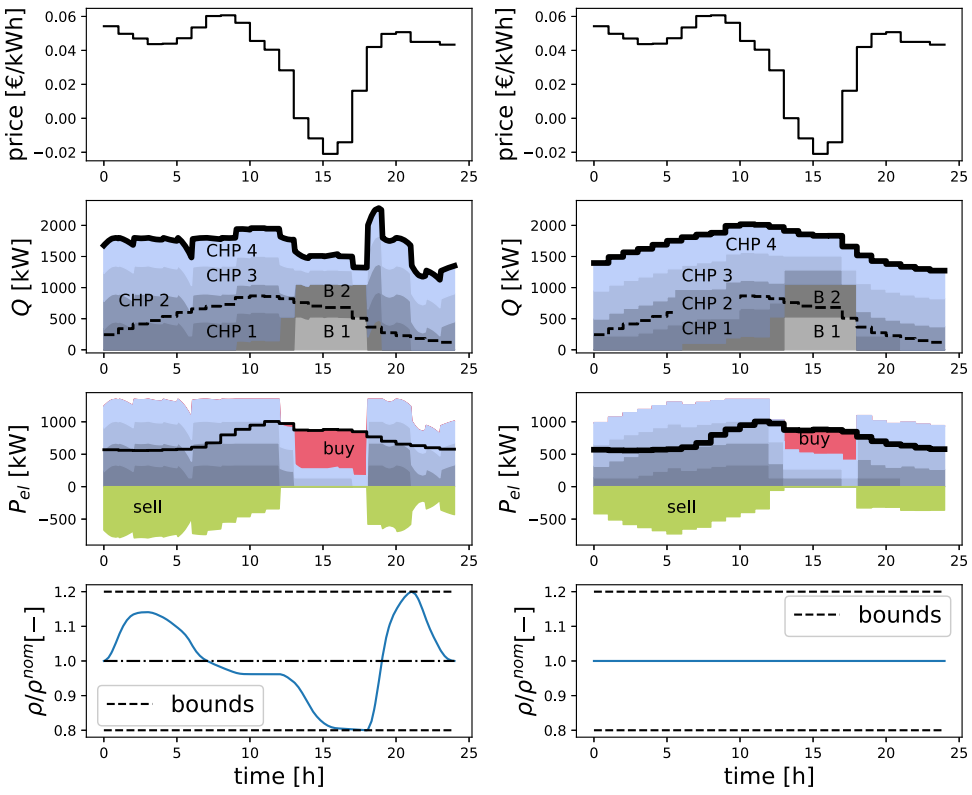

Fig. 11. Resulting schedule for the flexible process performing demand response (left) and the flexible process being operated in steady-state (right). Top: electricity price. Second row: heat supplied by the 4 combined heat and power plants (CHP1-CHP4) and the two boilers (B1, B2). The inflexible heat demand is shown as dashed black line and the total heat demand as bold black line. Third row: Electricity generated by CHP1 - CHP4, sold electricity to the grid, and electricity bought from the grid. The inflexible electricity demand is shown as black line. Bottom: Production rate ρ.

could be applied to the case of processes with two production rates ρ_1 and ρ_2, where the process model from Eq. (4) changes to $\dot{\mathbf{x}} = \mathbf{f}(\mathbf{x}, \mathbf{u}, \rho_1, \rho_2)$. In that case, there would be two ramping state vectors $\boldsymbol{\varphi}_1$ and $\boldsymbol{\varphi}_2$ and two ramping degrees of freedom ν_1 and ν_2. In general, the ramping degrees of freedom ν_1, ν_2 are limited by both ramping state vectors $\boldsymbol{\varphi}_1$, $\boldsymbol{\varphi}_2$ and also influence each other. Thus, the ramping limits read:

$$\nu_1^{\min}(\boldsymbol{\varphi}_1, \boldsymbol{\varphi}_2, \nu_2) \leq \nu_1 \leq \nu_1^{\max}(\boldsymbol{\varphi}_1, \boldsymbol{\varphi}_2, \nu_2) \tag{18}$$

$$\nu_2^{\min}(\boldsymbol{\varphi}_1, \boldsymbol{\varphi}_2, \nu_1) \leq \nu_2 \leq \nu_2^{\max}(\boldsymbol{\varphi}_1, \boldsymbol{\varphi}_2, \nu_1) \tag{19}$$

In principle, our dynamic ramping approach can also be applied to more than two scheduling-relevant variables. However, increasing the number of scheduling-relevant variables also increases the number of arguments entering the functions $\nu_i^{\min}(\cdot)$, $\nu_i^{\max}(\cdot)$. Thus, a piecewise affine approximation of the ramping limits $\nu_i^{\min}(\cdot)$, $\nu_i^{\max}(\cdot)$ might require many binaries and lead to a high computational burden.

The present work focuses on demand response applications where the production rate ρ is the main scheduling-relevant variable. However, it is straightforward to adapt the approach to cases where a different variable is scheduling-relevant. For example, in multi-product processes, the concentration may be varied to yield different products. Thus, the scheduling needs to account for the dynamics of the concentration during product transitions (Flores-Tlacuahuac and Grossmann, 2006; Baader et al., 2022c). Our approach can be transferred to such a multi-product process if the production rate ρ is replaced by the concentration.

The main limitation of our approach is the assumption of a flat process model. For non-flat process models, the ramping limits could still be derived as functions of all process states $\mathbf{x}$. However, it is not possible to find the coordinate transformation from the process states $\mathbf{x}$ to a transformed state vector $\boldsymbol{\Xi}$ as defined in Eq. (6), and thus, the ramping limits cannot be given as functions of the ramping state vector $\boldsymbol{\varphi}$ only. Hence, an extension to non-flat processes would be partly heuristic as the state vector $\mathbf{x}$ in the ramping limits would have to be approximated based on the ramping state $\boldsymbol{\varphi}$.

Another limitation of this work is that solving the equation system to derive the backtransformation requires a lot of manual effort, even though a computer algebra system is used as support. It is an open question to what extent our approach can be automated to enable the analysis of large-scale processes. Still, we do not consider this to be a significant restriction of our work as processes fulfilling our flatness assumption usually do not have too many states (Oldenburg and Marquardt, 2002): As inputs must be matched to outputs such that all states are covered (compare to the necessary graphical condition, e.g., Fig. 6), processes having much more states than inputs are usually not flat. Thus, our method will likely not be applicable to large-scale process models with hundreds of states. However, our approach seems applicable for flat process models with a number of states in the low double-digit range. As stated at the beginning of Section 4, we only reduced the textbook example by Christofides et al. (2011) from 9 states to 6 to ease the readability of the paper. Still, in a previous version, we considered the original version with 9 states and could find the inverse transformation easily using computer algebra. In future work, our approach could be coupled with model-order reduction approaches that derive a low-order representation of the process dynamics for the slow time scale (Baldea and Daoutidis, 2012). Even if the full-scale process model is not flat, the low-order dynamics relevant for scheduling optimization might be.

6. Conclusion

Dynamic ramping constraints simplify the simultaneous demand response scheduling optimization of production processes and their energy systems compared to an optimization considering the full-order

process model. Still, dynamic ramping constraints can capture more flexibility than traditional static ramping constraints as they allow high-order dynamics and non-constant ramp limits. In this paper, we extend our method to rigorously derive dynamic ramping constraints from input-state linearizable single-input single-output (SISO) processes (Baader et al., 2022a) to flat multi-input multi-output (MIMO) processes. In the MIMO case, dynamic ramping constraints reduce the problem dimensionality by coupling all flat outputs with the production rate. In our case study, a system with 6 states and 5 degrees of freedom is reduced to 2 states and one degree of freedom. Additionally, we demonstrate that an operational strategy can be chosen for flat outputs such that the steady-state production points are optimal, e.g., with respect to energy consumption.

Our case study demonstrates that dynamic ramping constraints allow for finding DR schedules for flexible processes and multi-energy systems that substantially reduce energy costs compared to a steady-state operation. Even though discrete on/off-decisions in the multi-energy system add to the computational complexity, the problem can be solved within the time limit for online scheduling.

Overall, dynamic ramping constraints allow bridging the gap between nonlinear process models and simplified process representations suitable for real-time scheduling optimization.

Nomenclature

Abbreviations

CHP	Combined heat and power plant
CSTR	Continuous stirred tank reactor
DR	Demand response
DRC	Dynamic ramping constraint
MIDO	Mixed-integer dynamic optimization
MILP	Mixed-integer linear program
MIMO	Multi-input multi-output
MINLP	Mixed-integer nonlinear program
SISO	Single-input single-output

Greek symbols

α	Integer number (compare to assumption 3a)
α_K	Relative volatility of component K
β	Integer number (compare to assumption 3b)
γ	Integer number (compare to assumption 3b)
δ	Order of dynamic ramping constraint
ζ	Integer number
κ	Integer number (compare to assumption 3a)
ν	Ramping degree of freedom
$\boldsymbol{\Xi}$	Transformed state vector
ξ	Flat output
π	Operating strategy
ρ	Production rate
ϱ_F	Density
$\boldsymbol{\Phi}$	Objective
ϕ	Transformation to flat output
$\boldsymbol{\varphi}$	Ramping state vector
ψ	Backtransformation from flat output

Latin symbols

a	Coefficient
b	Parameter
C	Coverage
C_p	Heat capacity
c	Concentration
E	Activation energy
F	Flow rate
f	Nonlinear function
H	Enthalpy
k	Reaction constant
m	Number of control inputs
n	Number of states
P	Power
Q	Heat flow
R	Gas constant
T	Temperature
t	Time
u	Control input
V	Volume
v	Vertex
x	State
z	Binary variable

Subscripts

0	Feed
1	Reactor
2	Flash
A	Component A
B	Component B or bottom
C	Component C
dem	Demand
el	Electric
f	Final time
p	Purge
s	Steady-state
V	Vaporization

Superscripts

max	Maximum
min	Minimum
nom	Nominal

CRediT authorship contribution statement

Florian Joseph Baader: Conceptualization, Methodology, Software, Investigation, Validation, Visualization, Writing – original draft. **Philipp Althaus:** Conceptualization, Writing – review & editing. **André Bardow:** Funding acquisition, Conceptualization, Supervision, Writing – review & editing. **Manuel Dahmen:** Conceptualization, Supervision, Writing – review & editing.

Declaration of competing interest

The authors declare that they have no known competing financial interests or personal relationships that could have appeared to influence the work reported in this paper.

Data availability

No data was used for the research described in the article.

Acknowledgments

This work was supported by the Helmholtz Association, Germany under the Joint Initiative “Energy System Integration”. AB and FB also received support from the Swiss Federal Office of Energy through the project “SWEET PATHFNDR”.

Appendix A. Supplementary data with illustrative examples and case study details

Supplementary material related to this article can be found online at https://doi.org/10.1016/j.compchemeng.2023.108171.

References

Adamson, R., Hobbs, M., Silcock, A., Willis, M.J., 2017. Integrated real-time production scheduling of a multiple cryogenic air separation unit and compressor plant. Comput. Chem. Eng. 104, 25–37. http://dx.doi.org/10.1016/j.compchemeng.2017.04.001.

Adamy, J., 2014. Nichtlineare Systeme Und Regelungen. Springer Vieweg, http://dx.doi.org/10.1007/978-3-642-45013-6.

Adeniran, A.A., Ferik, S.E., 2017. Modeling and identification of nonlinear systems: A review of the multimodel approach—Part 1. IEEE Trans. Syst. Man Cybern.: Syst. 47 (7), 1149–1159. http://dx.doi.org/10.1109/TSMC.2016.2560147.

Baader, F.J., Althaus, P., Bardow, A., Dahmen, M., 2022a. Dynamic ramping for demand response of processes and energy systems based on exact linearization. J. Process Control 118, 218–230. http://dx.doi.org/10.1016/j.jprocont.2022.08.017.

Baader, F.J., Bardow, A., Dahmen, M., 2022b. MILP formulation for dynamic demand response of electrolyzers. In: Yamashita, Y., Kano, M. (Eds.), 14th International Symposium on Process Systems Engineering. In: Computer Aided Chemical Engineering, vol. 49, Elsevier, pp. 391–396. http://dx.doi.org/10.1016/B978-0-323-85159-6.50065-8.

Baader, F.J., Bardow, A., Dahmen, M., 2022c. Simultaneous mixed-integer dynamic scheduling of processes and their energy systems. AIChE J. e17741. http://dx.doi.org/10.1002/aic.17741.

Baldea, M., Daoutidis, P., 2012. Dynamics and Nonlinear Control of Integrated Process Systems. In: Cambridge Series in Chemical Engineering, Cambridge University Press, http://dx.doi.org/10.1017/CBO9780511978760.

Baldea, M., Du, J., Park, J., Harjunkoski, I., 2015. Integrated production scheduling and model predictive control of continuous processes. AIChE J. 61 (12), 4179–4190. http://dx.doi.org/10.1002/aic.14951.

Baldea, M., Harjunkoski, I., 2014. Integrated production scheduling and process control: A systematic review. Comput. Chem. Eng. 71, 377–390. http://dx.doi.org/10.1016/j.compchemeng.2014.09.002.

Biegler, L.T., 2010. Nonlinear Programming: Concepts, Algorithms, and Applications to Chemical Processes. Society for Industrial and Applied Mathematics, http://dx.doi.org/10.1137/1.9780898719383.

Breiman, L., 1993. Hinging hyperplanes for regression, classification, and function approximation. IEEE Trans. Inform. Theory 39 (3), 999–1013. http://dx.doi.org/10.1109/18.256506.

Burnak, B., Katz, J., Diangelakis, N.A., Pistikopoulos, E.N., 2018. Simultaneous process scheduling and control: A multiparametric programming-based approach. Ind. Eng. Chem. Res. 57 (11), 3963–3976. http://dx.doi.org/10.1021/acs.iecr.7b04457.

Carrion, M., Arroyo, J.M., 2006. A computationally efficient mixed-integer linear formulation for the thermal unit commitment problem. IEEE Trans. Power Syst. 21 (3), 1371–1378. http://dx.doi.org/10.1109/TPWRS.2006.876672.

Christofides, P.D., Liu, J., La Muñoz de Peña, D., 2011. Networked and Distributed Predictive Control. Springer London, London, http://dx.doi.org/10.1007/978-0-85729-582-8.

Diangelakis, N.A., Burnak, B., Pistikopoulos, E.N., 2017. A Multi-Parametric Programming Approach for the Simultaneous Process Scheduling and Control Application to a Domestic Cogeneration Unit. Foundations of Computer Aided Process Operations/Chemical Process Control (FOCAPO/CPC), https://folk.ntnu.no/skoge/prost/proceedings/focapo-cpc-2017/FOCAPO-CPC%202017%20Contributed%20Papers/72_FOCAPO_Contributed.pdf (accessed 06 January 2022).

Dias, L.S., Ierapetritou, M.G., 2016. Integration of scheduling and control under uncertainties: Review and challenges. Chem. Eng. Res. Des. 116, 98–113. http://dx.doi.org/10.1016/j.cherd.2016.10.047.

Du, J., Park, J., Harjunkoski, I., Baldea, M., 2015. A time scale-bridging approach for integrating production scheduling and process control. Comput. Chem. Eng. 79, 59–69. http://dx.doi.org/10.1016/j.compchemeng.2015.04.026.

Flamm, B., Peter, C., Büchi, F.N., Lygeros, J., 2021. Electrolyzer modeling and real-time control for optimized production of hydrogen gas. Appl. Energy 281, 116031. http://dx.doi.org/10.1016/j.apenergy.2020.116031.

Fliess, M., Lévine, J., Martin, P., Rouchon, P., 1995. Flatness and defect of nonlinear systems: Introductory theory and examples. Internat. J. Control 61, 13–27. http://dx.doi.org/10.1080/00207179508921959.

Flores-Tlacuahuac, A., Grossmann, I.E., 2006. Simultaneous cyclic scheduling and control of a multiproduct CSTR. Ind. Eng. Chem. Res. 45 (20), 6698–6712. http://dx.doi.org/10.1021/ie051293d.

Grimstad, B., Andersson, H., 2019. ReLu networks as surrogate models in mixed-integer linear programs. Comput. Chem. Eng. 131, 106580. http://dx.doi.org/10.1016/j.compchemeng.2019.106580.

Gurobi Optimization, L., 2021. Gurobi optimizer reference manual. http://www.gurobi.com (accessed 09 February 2021).

Harjunkoski, I., Maravelias, C.T., Bongers, P., Castro, P.M., Engell, S., Grossmann, I.E., Hooker, J., Méndez, C., Sand, G., Wassick, J., 2014. Scope for industrial applications of production scheduling models and solution methods. Comput. Chem. Eng. 62, 161–193. http://dx.doi.org/10.1016/j.compchemeng.2013.12.001.

Hart, W.E., Laird, C.D., Watson, J.-P., Woodruff, D.L., Hackebeil, G.A., Nicholson, B.L., Siirola, J.D., 2017. Pyomo–Optimization Modeling in Python, Vol. 67, second ed. Springer Science & Business Media.

Hart, W.E., Watson, J.-P., Woodruff, D.L., 2011. Pyomo: Modeling and solving mathematical programs in Python. Math. Program. Comput. 3 (3), 219–260. http://dx.doi.org/10.1007/s12532-011-0026-8.

Hoffmann, C., Hübner, J., Klaucke, F., Milojević, N., Müller, R., Neumann, M., Weigert, J., Esche, E., Hofmann, M., Repke, J.-U., Schomäcker, R., Strasser, P., Tsatsaronis, G., 2021. Assessing the realizable flexibility potential of electrochemical processes. Ind. Eng. Chem. Res. 60 (37), 13637–13660. http://dx.doi.org/10.1021/acs.iecr.1c01360.

Jogwar, S.S., Baldea, M., Daoutidis, P., 2009. Dynamics and control of process networks with large energy recycle. Ind. Eng. Chem. Res. 48 (13), 6087–6097. http://dx.doi.org/10.1021/ie801050b.

Kämper, A., Holtwerth, A., Leenders, L., Bardow, A., 2021. AutoMoG 3D: Automated data-driven model generation of multi-energy systems using hinging hyperplanes. Front. Energy Res. 9, 430. http://dx.doi.org/10.3389/fenrg.2021.719658.

Kelley, M.T., Pattison, R.C., Baldick, R., Baldea, M., 2018. An efficient MILP framework for integrating nonlinear process dynamics and control in optimal production scheduling calculations. Comput. Chem. Eng. 110, 35–52. http://dx.doi.org/10.1016/j.compchemeng.2017.11.021.

Leenders, L., Bahl, B., Hennen, M., Bardow, A., 2019. Coordinating scheduling of production and utility system using a Stackelberg game. Energy 175, 1283–1295. http://dx.doi.org/10.1016/j.energy.2019.03.132.

Lueg, L., Grimstad, B., Mitsos, A., Schweidtmann, A.M., 2021. reluMIP: Open source tool for MILP optimization of ReLu neural networks. http://dx.doi.org/10.5281/zenodo.5601907.

Meurer, A., Smith, C.P., Paprocki, M., Čertík, O., Kirpichev, S.B., Rocklin, M., Kumar, A., Ivanov, S., Moore, J.K., Singh, S., Rathnayake, T., Vig, S., Granger, B.E., Muller, R.P., Bonazzi, F., Gupta, H., Vats, S., Johansson, F., Pedregosa, F., Curry, M.J., Terrel, A.R., Roučka, Š., Saboo, A., Fernando, I., Kulal, S., Cimrman, R., Scopatz, A., 2017. SymPy: symbolic computing in Python. PeerJ Comput. Sci. 3, e103. http://dx.doi.org/10.7717/peerj-cs.103.

Mitra, S., Grossmann, I.E., Pinto, J.M., Arora, N., 2012. Optimal production planning under time-sensitive electricity prices for continuous power-intensive processes. Comput. Chem. Eng. 38, 171–184. http://dx.doi.org/10.1016/j.compchemeng.2011.09.019.

Nicholson, B., Siirola, J.D., Watson, J.-P., Zavala, V.M., Biegler, L.T., 2018. Pyomo.dae: A modeling and automatic discretization framework for optimization with differential and algebraic equations. Math. Program. Comput. 10 (2), 187–223. http://dx.doi.org/10.1007/s12532-017-0127-0.

Oldenburg, J., Marquardt, W., 2002. Flatness and higher order differential model representations in dynamic optimization. Comput. Chem. Eng. 26 (3), 385–400. http://dx.doi.org/10.1016/S0098-1354(01)00752-9.

Pattison, R.C., Touretzky, C.R., Johansson, T., Harjunkoski, I., Baldea, M., 2016. Optimal process operations in fast-changing electricity markets: Framework for scheduling with low-order dynamic models and an air separation application. Ind. Eng. Chem. Res. 55 (16), 4562–4584. http://dx.doi.org/10.1021/acs.iecr.5b03499.

Rothfuß, R., 1997. Anwendung Der Flachheitsbasierten Analyse Und Regelung Nichtlinearer Mehrgröß Ensysteme. VDI-Verl., Düsseldorf.

Rothfuß, R., Rudolph, J., Zeitz, M., 1996. Flatness based control of a nonlinear chemical reactor model. Automatica 32 (10), 1433–1439. http://dx.doi.org/10.1016/0005-1098(96)00090-8.

Sass, S., Faulwasser, T., Hollermann, D.E., Kappatou, C.D., Sauer, D., Schütz, T., Shu, D.Y., Bardow, A., Gröll, L., Hagenmeyer, V., Müller, D., Mitsos, A., 2020. Model compendium, data, and optimization benchmarks for sector-coupled energy systems. Comput. Chem. Eng. 135, 106760. http://dx.doi.org/10.1016/j.compchemeng.2020.106760.

Schäfer, P., Daun, T.M., Mitsos, A., 2020. Do investments in flexibility enhance sustainability? A simulative study considering the German electricity sector. AIChE J. 66 (11), e17010. http://dx.doi.org/10.1002/aic.17010.

Schulze, M., Schenkendorf, R., 2020. Robust model selection: Flatness-based optimal experimental design for a biocatalytic reaction. Processes 8 (2), http://dx.doi.org/10.3390/pr8020190.

Schweidtmann, A.M., Weber, J.M., Wende, C., Netze, L., Mitsos, A., 2021. Obey validity limits of data-driven models through topological data analysis and one-class classification. Opt. Eng. http://dx.doi.org/10.1007/s11081-021-09608-0.

Simkoff, J.M., Baldea, M., 2020. Stochastic scheduling and control using data-driven nonlinear dynamic models: Application to demand response operation of a chlor-alkali plant. Ind. Eng. Chem. Res. http://dx.doi.org/10.1021/acs.iecr.9b06866.

Unger, J., Kröner, A., Marquardt, W., 1995. Structural analysis of differential-algebraic equation systems—theory and applications. Comput. Chem. Eng. 19 (8), 867–882. http://dx.doi.org/10.1016/0098-1354(94)00094-5.

Virtanen, P., Gommers, R., Oliphant, T.E., Haberland, M., Reddy, T., Cournapeau, D., Burovski, E., Peterson, P., Weckesser, W., Bright, J., van der Walt, S.J., Brett, M., Wilson, J., Millman, K.J., Mayorov, N., Nelson, A.R.J., Jones, E., Kern, R., Larson, E., Carey, C.J., Polat, İ., Feng, Y., Moore, E.W., VanderPlas, J., Laxalde, D., Perktold, J., Cimrman, R., Henriksen, I., Quintero, E.A., Harris, C.R., Archibald, A.M., Ribeiro, A.H., Pedregosa, F., van Mulbregt, P., SciPy 1.0 Contributors, 2020. SciPy 1.0: Fundamental Algorithms for Scientific Computing in Python. Nature Methods 17, 261–272. http://dx.doi.org/10.1038/s41592-019-0686-2.

Voll, P., Klaffke, C., Hennen, M., Bardow, A., 2013. Automated superstructure-based synthesis and optimization of distributed energy supply systems. Energy 50, 374–388. http://dx.doi.org/10.1016/j.energy.2012.10.045.

Zhang, Q., Grossmann, I.E., 2016. Planning and scheduling for industrial demand side management: Advances and challenges. In: Martín, M.M. (Ed.), Alternative Energy Sources and Technologies. In: Engineering, Springer, Switzerland, pp. 383–414. http://dx.doi.org/10.1007/978-3-319-28752-2_14.

Zhang, Q., Grossmann, I.E., Sundaramoorthy, A., Pinto, J.M., 2016. Data-driven construction of convex region surrogate models. Opt. Eng. 17 (2), 289–332. http://dx.doi.org/10.1007/s11081-015-9288-8.

Zhou, D., Zhou, K., Zhu, L., Zhao, J., Xu, Z., Shao, Z., Chen, X., 2017. Optimal scheduling of multiple sets of air separation units with frequent load-change operation. Sep. Purif. Technol. 172, 178–191. http://dx.doi.org/10.1016/j.seppur.2016.08.009.